Nanoscale Advances

ROYAL SOCIETY OF CHEMISTRY

PAPER

View Article Online
View Journal | View Issue

Cite this: *Nanoscale Adv.*, 2020, **2**, 4627

A highly efficient fog harvester of electrospun permanent superhydrophobic–hydrophilic polymer nanocomposite fiber mats

Md. Nizam Uddin, Fenil J. Desai, Muhammad M. Rahman and Ramazan Asmatulu*

To address the worldwide issue of water scarcity, which is threatening our sustainable economic development and ecological security, an efficient water-collecting surface with fast-capturing capability and easy drainage is essential. Inspired by the fog-harvesting capability of *Stenocara* beetles in the Namib Desert, this study presents an easy method for fabricating flexible, permanent, electrospun superhydrophobic–hydrophilic polyacrylonitrile (PAN) and poly(methyl methacrylate) (PMMA) nanocomposite fiber mats for atmospheric fog water harvesting. This combination of a hydrophobic PAN domain and hydrophilic nanomaterials causes water to condense on the hydrophilic micro and nanoparticles and roll off the hydrophobic nanofibers. By adjusting the proportion of micro and nanomaterials, we can tune the fog water harvesting efficiency. The superhydrophobic–hydrophilic nanocomposite fibers are fabricated with various proportions of titanium dioxide (TiO_2) nanoparticles and aluminum (Al) microparticles using the electrospinning technique followed by stabilization and carbonization to remove all non-carbonaceous materials from the fiber structures. The fiber morphology, surface hydrophobicity, crystal structure, and fog-harvesting performance of the nanocomposite fibers were investigated. A water contact angle of 154.8° was achieved with the addition of a 10% inclusion of combined micro- and nanoparticles. The experimental tests of these nanocomposites demonstrated the feasibility of the freshwater production with a daily water productivity of more than 1.49 liter m^{-2} of the nanocomposites. It is estimated that the material cost of making such nanocomposites to supply minimum daily water consumption for a household with 2 members (*i.e.*, 6 liters) is only $4.96 (USD). These nanocomposites are cheap and affordable, and require no additional input of energy, and are especially suitable for clean water production in arid areas. This work offers a very feasible and novel tool to achieve the mass production of water-harvesting materials.

Received 29th June 2020
Accepted 20th August 2020

DOI: 10.1039/d0na00529k

rsc.li/nanoscale-advances

1. Introduction

The global water shortage issue has led to the development of water-capturing technology since the 20th century, especially in countries with arid and semi-arid regions. The rainfall in such areas is limited, so animals and plants obtain water from atmospheric fog, moisture, *etc.* However, atmospheric fog represents a substantial freshwater source. The atmosphere contains 37.5 million billion gallons of water in the invisible vapor phase. Approximately one billion people are suffering to gain access to clean water sources around the globe.[1] By 2025, around 2.4 billion people will be living in areas with absolute water scarcity, as reported by the United Nations Convention to Combat Desertification.[2] Also, industrial growth, population growth, urbanization, depletion of water resources, deforestation, and many other factors contribute to the water crisis issue. Therefore, engineers and scientists are challenged with finding economically feasible and viable water resources to solve the problem. In some Asian, African, and Latin American countries, alternative methods such as rain and groundwater harvesting, cloud seeding, and desalination are already being used to produce pure water for drinking, agricultural, gardening, medical, industrial, and other purposes.[3] In some parts of Europe and the Middle East, desalination is the only source for reclaiming fresh water. However, these methods are pricey, with a high operational cost. Harvesting fog water with high efficiency is a charming approach to relieve the menace of water deficiency.

In nature, many animals and plants have special wetting properties as a result of the uniquely designed micro- and nanoscale structural features on their surfaces.[4] What these species use to collect water from fog and dew in a desert provides a new insight to obtain water. For example, in the Namib Desert, the *Stenocara* beetle harvests water directly from the fog and mist, dropping water into its mouth at a tilted angle. This beetle's carapace has a combination of hydrophilic bumps and a hydrophobic surface that facilitates water collection from

Department of Mechanical Engineering, Wichita State University, 1845 Fairmount Street, Wichita, KS 67260, USA. E-mail: ramazan.asmatulu@wichita.edu

fog.[5] When a fog droplet carried by wind meets the hydrophilic bumps, these bumps capture the droplet which coalesces, while the hydrophobic surface drains the water directly into the beetle's mouth. Cribellate spiders use silk with spindle-knots and a joint structure that provides wettability and curvature gradients to collect water from the atmosphere.[4] In the past decade, extensive research on mimicking nature has been done to develop a cleaner and efficient way of capturing atmospheric water to manage the freshwater scarcity issue.[6–10] For efficient fog harvesting, the hydrophobicity and hydrophilicity of collector materials significantly affect their fast water capturing and easy drainage properties. Moreover, superhydrophobic surfaces have other advantages such as self-cleaning, stain resistance, drag reduction, and oil spill separation.[11–15]

Very few studies have focused on the fabrication of permanent superhydrophobic polymer nanocomposite fibers using nanotechnology.[16–18] A bioinspired hydrophilic–superhydrophobic patterned hybrid surface was fabricated for efficient fog collection by Wang *et al.* in 2015.[19] The hybrid surface was composed of a superhydrophobically modified metal-based gauze attached to the surface of a hydrophilic polystyrene (PS) flat sheet. A higher collection efficiency of about 159 mg cm^{-2} h^{-1} was achieved with the hydrophilic–superhydrophobic patterned hybrid surface. In 2013, Lalia *et al.* fabricated hydrophobic poly(vinylidene fluoride-*co*-hexafluoropropylene) PVDF–HFP nanowebs using the electrospinning process and impregnated this nanoweb with lubricants (total quartz oil and Krytox 1506) to investigate the efficiency of fog collection.[20] The lubricant-impregnated nanomats reduced the contact angle hysteresis and improved the water collection efficiency. In addition, the lubricant-impregnated nanomats had less oil drainage from the surface along with shedding water. A fog-harvesting efficiency of 118 mg cm^{-2} h^{-1} was achieved with the lubricant impregnated nanomats. PVDF spindle-knot fibers were fabricated based on the breaking-up of the droplets of a solution film (Rayleigh instability break-up droplets) and water-collecting ability in a humid environment.[21] The spindle-knot fiber was comprised of multi-level spindle-knots that can generate continuous gradients of surface energy and different Laplace pressures. However, spindle-knot fibers have shown much higher water collection efficiency than normal uniform fibers. Besides, the effect of different fiber cross-sections and surface structures on fog collection has been analyzed to optimize fog-collecting meshes.[22] In another study, fourteen polyethylene terephthalate (PET) fibers with different cross-sections and surface structures such as microgrooves were fabricated, and fog-collection efficiency was measured. It was observed that micro-grooved fiber surfaces increase the deposition efficiency, and the directional surface transport enhances the drainage efficiency, followed by improvement in the total fog-collection quantity. The cross-section and width of the fibers substantially influenced the droplet movement. The combination of a round cross-section (or a rectangular cross-sectional profile with round edges) with a micro-grooved hydrophilic surface and optimum diameter optimizes the collection efficiency.

A PVDF/expanded graphite (EG) composite was fabricated using electrospinning methodology, and its water-harvesting capability was investigated.[23] Bare PVDF fibers show a harvesting capacity of 103.1 mg cm^{-2} h^{-1}, whereas PVDF/EG has a harvesting capacity of 168.5 mg cm^{-2} h^{-1}. About 63.4% enhancement of the harvesting capacity was observed with the introduction of EG. After multi-cycle testing, the composite showed a similar morphology, wettability, and fog-harvesting performance, thereby indicating reusability for a longer period. Almasian *et al.* fabricated fluorinated superhydrophobic PAN nanofibers for investigating their fog-harvesting properties.[24] The synthesis process was optimized by varying the temperature, time, and amount of the fluoroamine compound. Synthesized PAN nanofibers had a water contact angle of 159° and low surface energy of 17.1 mN m^{-1}. The maximum fog-harvesting capacity of 335 mg cm^{-2} h^{-1} was obtained when the nanofibers were treated for 3 h at 95 °C, and the amount of the fluoroamine compound was 8% (w/w) in the modification process. The fluorinated nanofibers exhibited greater harvesting performance than untreated PAN nanofibers (31 mg cm^{-2} h^{-1}) because of the superhydrophobic nature of the fluorinated nanofibers.

Although plenty of methods have been developed to mimic the structure on the *Stenocara* beetles' back for water-harvesting, in areas where people are suffering for water and that are relatively poverty-stricken with underdeveloped regions, supplies and manufacturing facilities are inadequate. Therefore, issues still exist for easier fabrication, mass production, and processing of fog water harvesting materials. The study focusses on fabricating PAN and PMMA superhydrophobic–hydrophilic nanocomposite fiber mats with incorporated TiO_2 nanoparticles and Al microparticles and studying their fog water harvesting performance. The novelty of this work is that for the first time a highly efficient fog harvesting method was designed and developed using nanocomposite fibers, which is especially suitable for clean water production in arid areas.

2. Experimental

2.1. Materials

PAN (molecular weight, M_w 150 000 g mol^{-1}, T_g 95 °C) and PMMA (M_w 120 000 g mol^{-1}, T_g 99.0 °C) were purchased from Sigma-Aldrich (St. Louis, MO, USA). TiO_2 nanoparticles of an average particle size of 40 nm (anatase, 99.5%) and Al microparticles (99.7%, 10 μm) were both purchased from U.S. Research Nanomaterials Inc., TX, USA. All the materials used in this study were original without any modifications to the supplier specifications.

2.2. Fabrication of PAN/PMMA nanocomposite fiber mats

The nanocomposite fiber mats were fabricated using the electrospinning technique. Along with PAN and PMMA polymers, micro- and nanoparticles of Al and TiO_2 were sonicated by using a probe sonicator to produce a homogeneous polymer blend. Different concentrations of micro- and nanoparticles were used (0, 2.5, 5, and 10 wt%) to fabricate the PAN/PMMA nanocomposites. As shown in Fig. 1, to prepare a homogeneous polymer solution, PAN and PMMA were dissolved in DMF in

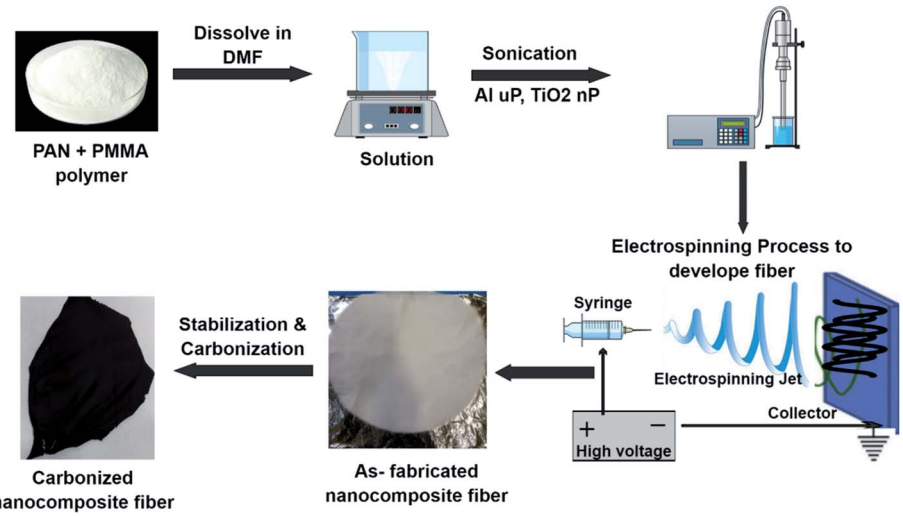

Fig. 1 Illustration of the fabrication process of electrospun PAN/PMMA nanocomposite fiber mats.

a ratio of 80 : 20 at 45 °C for 2 h. The ratio of PAN and PMMA was 25 : 75 percent by weight. Subsequently, the micro- and nanoparticles of Al and TiO_2 were added into the polymer solution and stirred for another 2 h followed by 20 min of probe sonication. The prepared solution was electrospun and then dried for 24 h in an open atmosphere. The electrospinning was conducted at 25 kV and a feed rate of 1 ml h^{-1}, and the distance between the tip and collector was 25 cm. The fabricated fibers were then stabilized and carbonized at 250 °C and 850 °C for 1 h in an oxygen and argon environment respectively.

2.3. Characterization of nanocomposite fibers

The water contact angles of the PAN/PMMA nanocomposite fiber mats were measured with a water contact angle goniometer (KSV Instruments Ltd., Model #CAM 100). The morphology of the fabricated nanocomposite fibers was characterized using scanning electron microscopy (SEM) (FEI Nova Nano SEM 450). A Mitutoyo 178-561-02A Surftest SJ-210 surface roughness tester was used to measure the surface roughness. The surface chemistry of the nanocomposite fibers was studied by Fourier-transform infrared spectroscopy (FTIR) (Thermo Scientific™ Nicolet™ iN10 infrared microscope) over a range of 3500–500 cm^{-1}. The structural properties of the nanocomposite fibers were evaluated by X-ray diffraction (XRD). Also, Cu Kα (λ = 0.15418 nm) radiation over a 2θ range of 10–70° was used for this analysis. The apparent crystallite thickness (L_c), the apparent layer-plane length parallel to the fiber axis (L_a), and the average interlayer spacing (d) were calculated using Bragg's and Scherrer's formulas. These formulas can be expressed, respectively, as:

$$d = \frac{\lambda}{2 \sin \theta} \quad (1)$$

$$L = \frac{k\lambda}{\beta \cos \theta} \quad (2)$$

where θ is the Bragg angle in degrees, λ is the wavelength of the X-ray used, and β is the full-width half-maximum of a given peak (rad).

3. Results and discussion

3.1. Characteristics of nanocomposite fibers

The FTIR spectra of the as fabricated and carbonized nanocomposite fibers are shown in Fig. 2. The PAN molecule is a linear arrangement of methyl (CH_3) and nitrile (C≡N) groups.[25] Some new compounds such as ketones, aldehydes, and carboxylic acids are formed during the stabilization process. However, in the carbonization process at high temperature, *i.e.*, 850 °C, all the volatile compounds are burnt out, leaving only carbon and hydrogen molecules in the carbon fiber structure. In the spectrum of the untreated fiber, the peak intensities at 987 and 1450 cm^{-1} are assigned to the aliphatic CH group vibration of different modes in CH_2 and CH respectively. The bands corresponding to 1150 and 1720 cm^{-1} are due to C–O and C=O stretching, and the bands corresponding to 1240 and 2360 cm^{-1} are due to C–N and C≡N stretching. The absorption peaks of C–O and C=O groups weaken gradually with the addition of Al microparticles and TiO_2 nanoparticles. As shown in (Fig. 2b), carbonization results in changes in the characteristic absorption peaks of the FTIR spectrum. Most importantly, almost all the strong peaks disappeared after carbonization. All the peaks disappeared, compared to those in the untreated PAN/PMMA fiber spectrum.

The average roughness of the carbonized nanocomposite fibers was measured. The average roughness of the PAN/PMMA fibers had the lowest roughness of 0.34 ± 0.02 μm and it was affected considerably by incorporating a combination of micro and nanomaterials. For 2.5, 5 and 10 wt% micro and nanomaterial inclusions, the average roughness of the nanocomposites was 0.49 ± 0.03, 0.94 ± 0.05 and 1.77 ± 0.04 μm respectively. The structural changes during the carbonization of the nanocomposite fibers were observed by XRD analysis

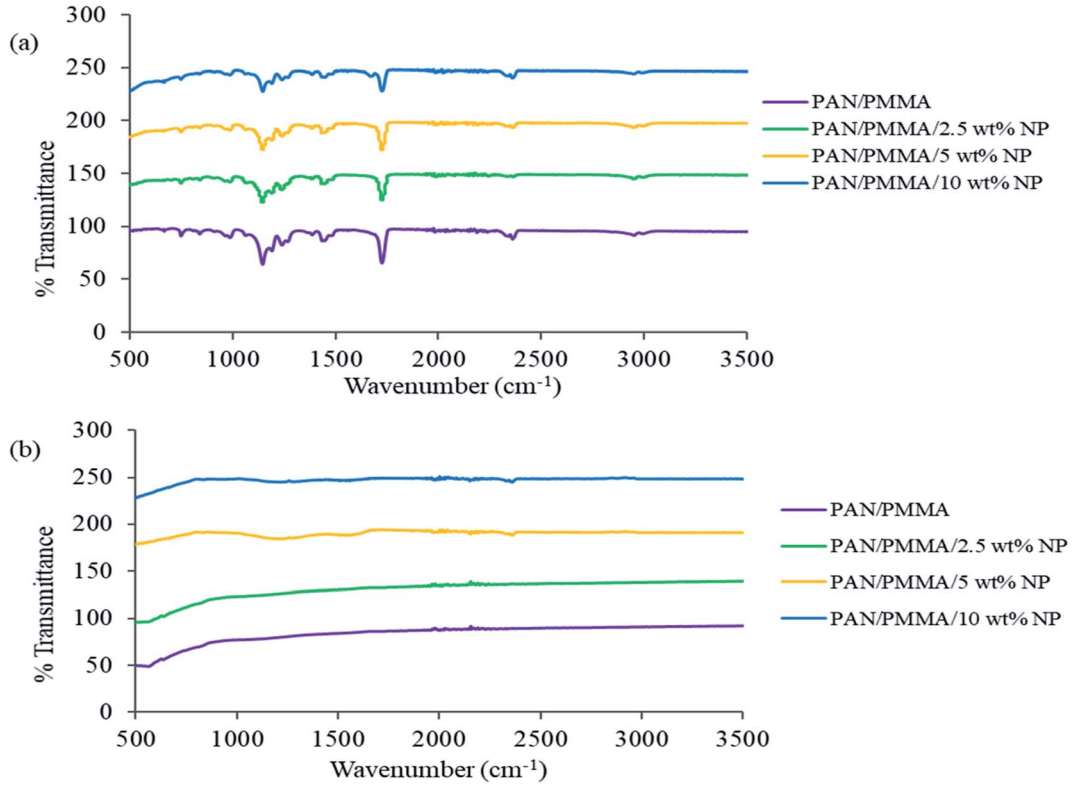

Fig. 2 FTIR spectra of the nanocomposite fibers: (a) as prepared and (b) after carbonization.

(Fig. 3). The broader XRD peak of the carbonized PAN/PMMA nanofibers is mainly due to the carbon peak ($2\theta \cong 24^\circ$) coming from the PAN polymer. The XRD peaks at 2θ of 25° (101 plane), 37° (103 plane), 48° (200 plane), 55° (211 plane) and 62° (002 plane) are typical of crystal TiO_2 nanoparticles,[26] while those at 37° (312 plane), 62° (511 plane) and 67° (440 plane) are typical crystal Al_2O_3 particle peaks.[27] The shape factor k is 0.89 for L_c and 1.84 for L_a, respectively.[28] Scherrer's equation was used to calculate the values of L_c (stacking height of layer planes) from the width of the (002) reflection. For the carbonized samples, the peaks shifted up with 5 wt% nanoparticles, from 21.85° to 25.45°, which approaches the graphite peak position, and diffraction also increased considerably. This shows that the atoms of carbon were rearranged in order and improved the crystalline structure in the fiber. The structural parameters determined by XRD for the carbonized PAN/PMMA nanocomposite are summarized in Table 1. Several chemical reactions such as cyclization, degradation, and cross-linking can occur when the PAN/PMMA fibers are heated at high temperatures, and the mechanism of the process is related to

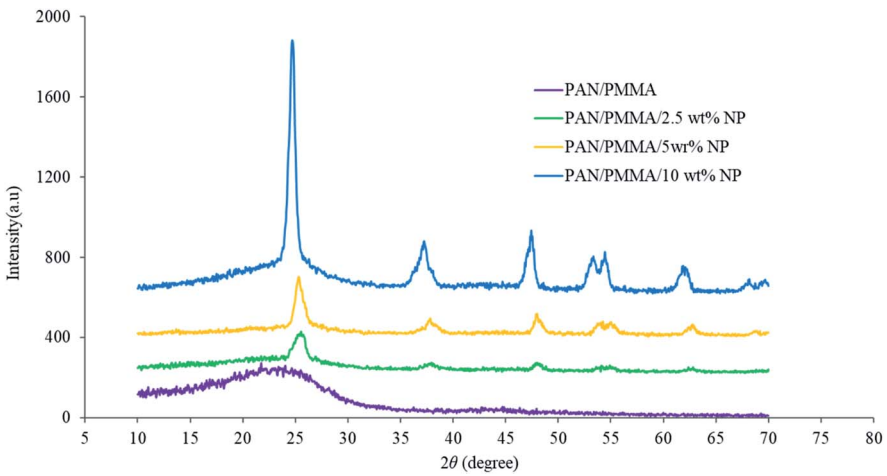

Fig. 3 XRD patterns of carbonized PAN/PMMA nanocomposites with various nanoparticle inclusions.

Table 1 Structural parameters determined by XRD for carbonized nanocomposite fibers with various nanoparticle inclusions

Nanocomposite fibers	$d_{(002)}$ (nm)	L_c (nm)	$L_c/d_{(002)}$
PAN/PMMA	0.35	1.01	0.027
PAN/PMMA/2.5 wt% NPs	0.36	4.83	13.80
PAN/PMMA/5 wt% NPs	0.35	7.46	21.31
PAN/PMMA/10 wt% NPs	0.36	10.80	30.0

the heating rate, polymer and type and nature of the inclusions.[29]

The EDX spectra of the as-fabricated and carbonized nanocomposite fibers are presented in Fig. 4. As can be seen in Fig. 4(a), the fibers fabricated without the addition of nanomaterials show a strong carbon peak (74.32%), which is mainly from the polymer structure. However, the carbonized fibers also exhibit a strong carbon peak (92.7%). Furthermore, the EDX spectrum of the nanocomposite fibers with nanoparticle inclusions demonstrates that fibers are mainly composed of carbon (C), aluminum (Al), titanium (Ti), oxygen (O), and gold (Au). One important observation here is that all the carbonized fibers exhibited a higher percentage of carbon than the as-fabricated fibers. The Ti and Al peaks are particularly observed from the EDX spectra of the nanocomposite fibers. The EDX spectra support the presence of Al microparticles and TiO_2 nanoparticles on the surface of the fiber as well as the embedding of nanoparticles in the electrospun nanocomposite fibers.

Fig. 5 and 6 illustrate the SEM images of the as-fabricated and carbonized nanocomposite fibers, respectively. As can be seen in Fig. 5, the randomly oriented porous PAN/PMMA nanocomposite fibers are composed of smooth outer surfaces and some beaded structures. However, the well-developed coarseness and roughness of the nanocomposite fibers with higher diameters were achieved when Al microparticles and TiO_2 nanoparticles were introduced. These hierarchical micro- and nanostructures on the surface of the fibers can provide enough roughness for superhydrophobicity. The average diameters of the as-fabricated nanocomposite fibers without inclusions were 470 nm, and 10 wt% inclusions were 1.3 μm. Moreover, the increase of the fiber diameter with the concentration of the nanoparticles could be attributed to the increase in the viscosity of the polymer solution. Also, solution properties such as viscosity, elasticity, conductivity, and surface tension greatly influence the transformation of the polymer solution into nanofibers. However, in the carbonized fibers, due to the melting/burning of PMMA, their morphology and structure were significantly altered.

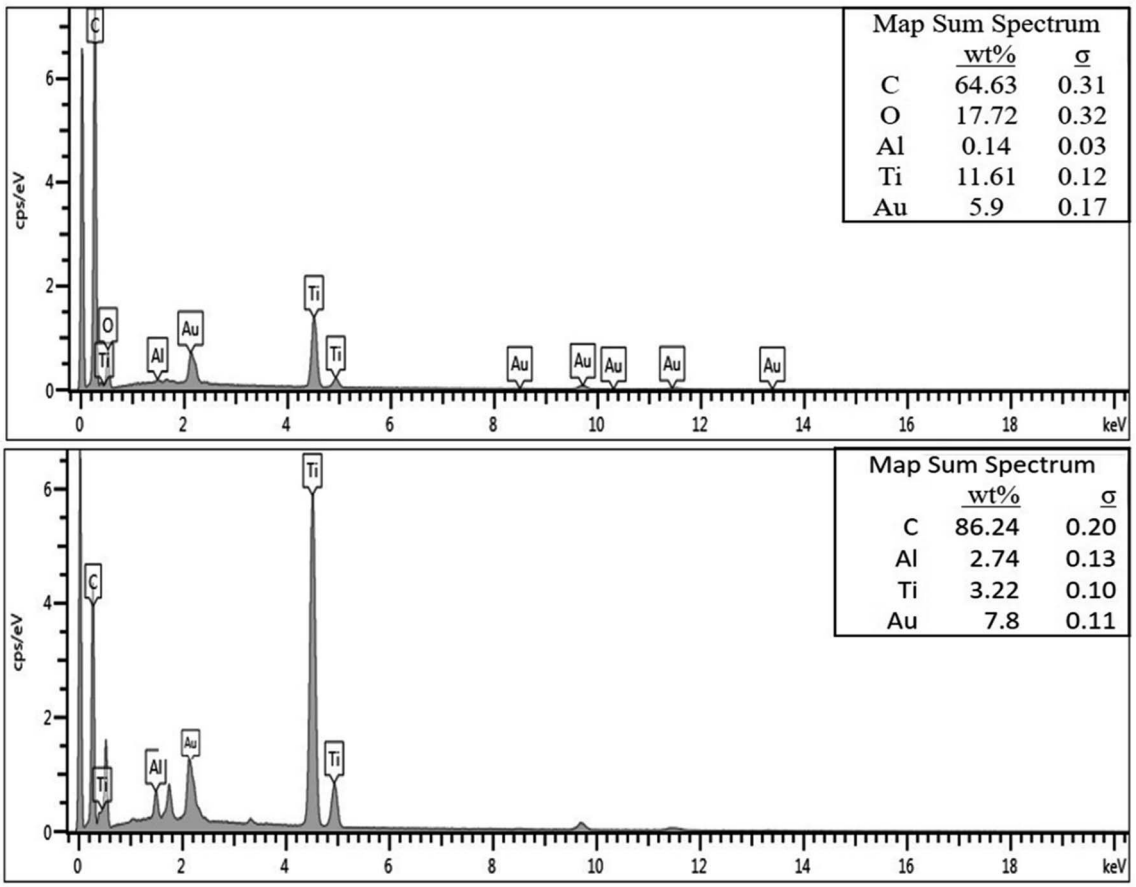

Fig. 4 EDX spectra of the as-fabricated (top) and carbonized (bottom) PAN/PMMA nanocomposites having 10 wt% Al microparticles and TiO_2 nanoparticles.

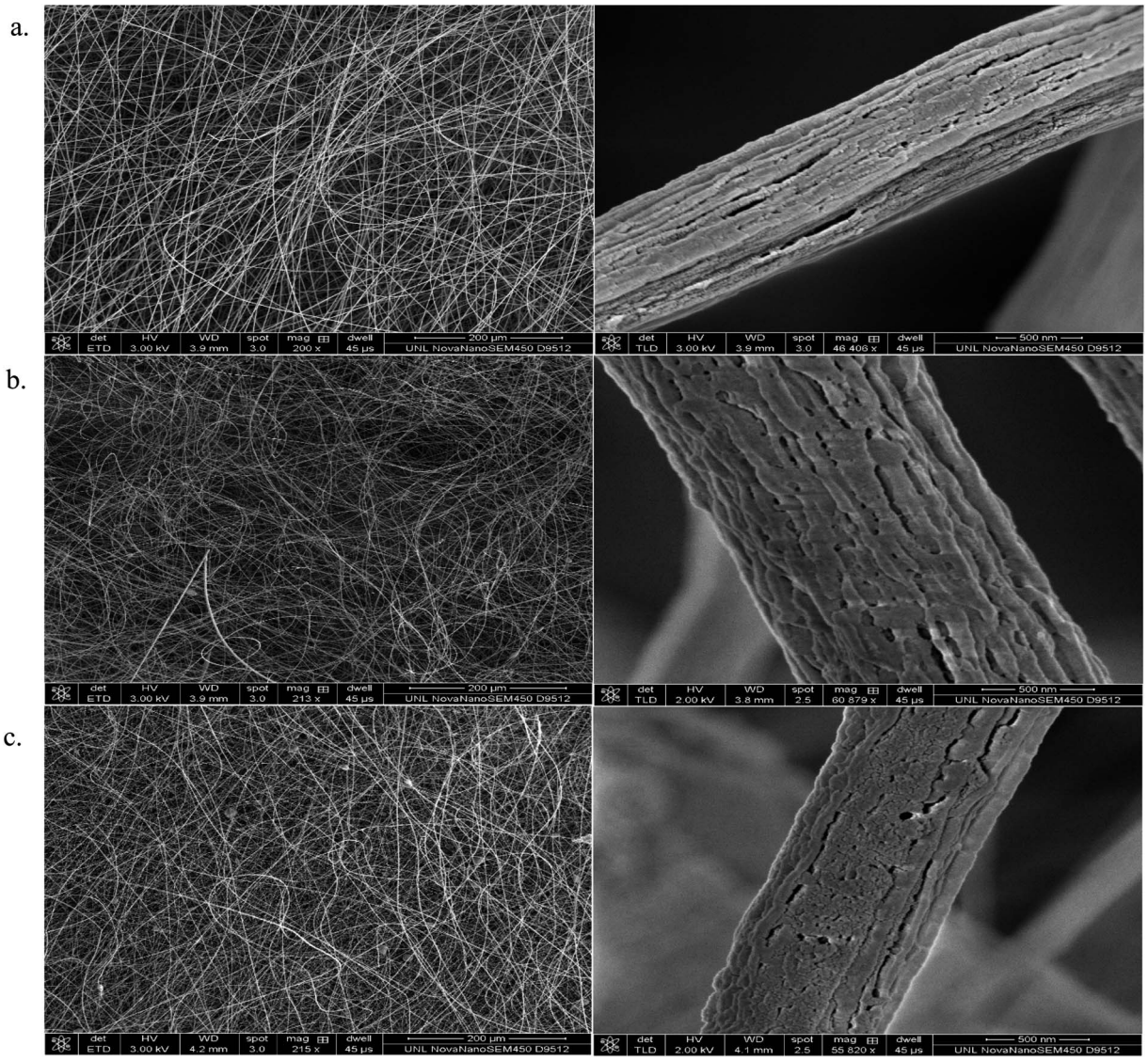

Fig. 5 SEM images of the electrospun as prepared PAN/PMMA nanocomposite fibers with: (a) 0 wt% NPs; (b) 5 wt% NPs; (c) 10 wt% NPs.

3.2. Hydrophobic characteristics of nanocomposite fiber mats

The chemical structure, surface geometrical structure, and consistency stimulate the characteristics of the hydrophobicity of a solid surface. The water contact angles of carbonized nanocomposites without and 10 wt% nanoparticle inclusions were about 130.86° and 154.8°, respectively, as shown in Fig. 7. Thus, the carbonized materials with 10 wt% nano- and microparticles show a superhydrophobic nature. The roll-off angle or sliding angle is below 10°, and in some surfaces, it is below 3°. Also, the composites were tested using 15 wt% TiO_2 and Al particles, but due to the higher viscosity, they could not be used for the electrospinning process.

The PAN/PMMA nanocomposite fibers were stabilized at 280 °C in an oxygen environment where PAN forms a ladder-like structure.[30] The stabilization process produces physically, chemically, and thermally stable nanocomposite fibers. Besides, during the stabilization process, the nanocomposite fibers are transformed from being thermoplastic to thermosetting, experiencing a reduction in diameters, and color change. Then the nanocomposite fibers were converted into carbon fibers by carbonizing at 850 °C in an argon atmosphere. This process significantly modifies the morphology, surface chemistry, and fiber structure. During this process, PMMA is burned out, creating porous fibers, and other non-carbonaceous compounds are released, and the polarity is eliminated by releasing the radicals attached to the main chain of the nanocomposite fibers. The surface roughness, along with porosity, produces a heterogeneous wetting state where the air is entrapped by water in the surface cavities,[31] thereby reducing the contact area between the water and the solid surface while increasing the contact area between the water and air. Therefore, the wettability of the solid surface is increased.

3.3. Fog harvesting of PAN/PMMA nanocomposite fiber mats

The three phenomena that influence the fog-harvesting efficiency involve capturing, collecting, and transporting. In the first stage, tiny fog droplets (diameter 1–40 µm) propelled by

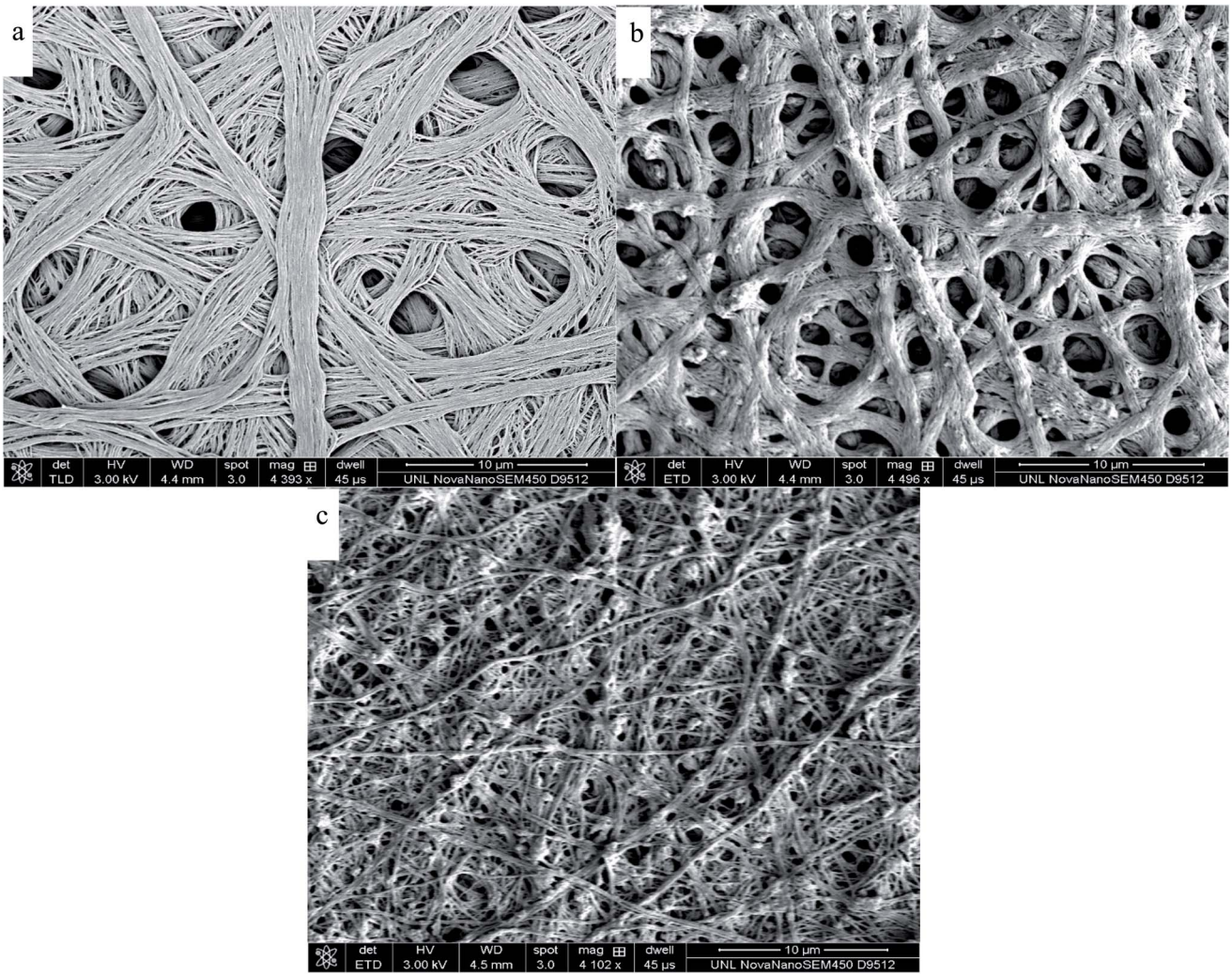

Fig. 6 SEM images of electrospun carbonized PAN/PMMA nanocomposite fibers: (a) PAN/PMMA; (b) PAN/PMMA/5 wt% NPs; (c) PAN/PMMA/10 wt% NPs.

wind must be captured onto the solid surfaces.[32,33] Herein, the harvesting efficiency depends on the wind flow velocity and hydrophilicity of the as-designed surfaces.[6] However, a tiny droplet may be captured by the surface, but improper collection can reduce the collection efficiency by evaporation of the captured tiny droplets, or wind can destroy the droplets. Therefore, the collection step is vital for a well-designed surface to achieve a high efficiency. Finally, in the transport stage, the droplets will roll off the surface due to gravity once they coalesce and grow large enough. In this step, the hydrophobicity of the solid surface and its area, as well as the tilted angle, are crucial factors. The whole process should be fast enough to avoid evaporation and subsequently enhance harvesting efficiency.

In this study, the fog harvesting performance of the PAN/PMMA nanocomposite fibers was evaluated by using a homemade test system. A conventional ultrasonic humidifier (Vicks, USA) was used to simulate natural fog. The humidifier produced a fog flow of 330 ml h^{-1} that was captured by the vertically placed nanofiber surfaces and used about 50 watts. The fog-collection behavior of the nanocomposite fibers was tested at controlled temperature and humidity. The temperature and humidity of the collection chamber were maintained at 19 $\pm$ 2 °C and 68 $\pm$ 3%, respectively, to minimize re-evaporation and to prevent droplet condensation. All the prepared samples with a size of 3 $\times$ 3 cm^2 were placed on a holder under ambient conditions. The distance between the humidifier and the sample was maintained at 5 cm. The sample was fixed vertically to the direction of the fog flow so that its surface was perpendicular to the horizontal plane. The scheme of the test system used to perform the fog collection experiment of the nanocomposite fibers is presented in Fig. 8. A clean beaker was placed under the sample to collect the water dripping from the sample. The amount of water harvested using the nanocomposite fibers was noted every 20 min for a total period of 60 min. Moreover, to observe the water condensation and coalescence process, a digital camera was used to capture the images.

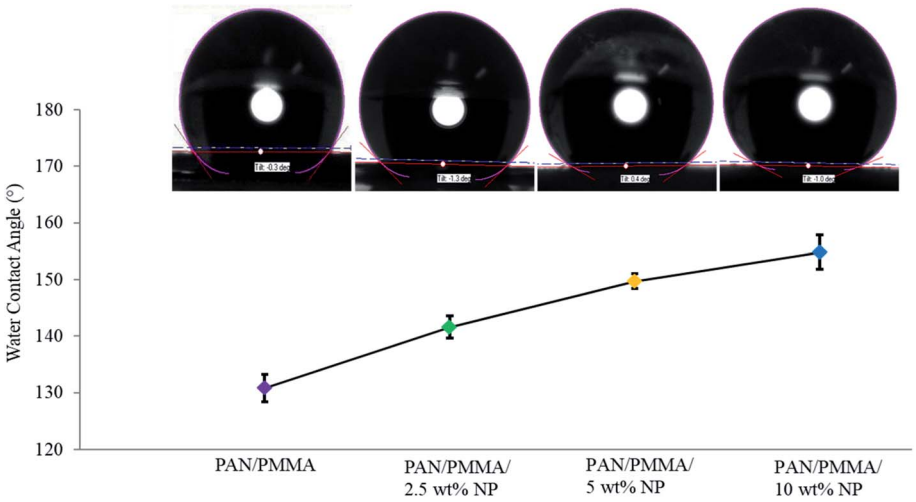

Fig. 7 The water contact angle of carbonized nanocomposite fibers with 0, 2.5, 5 and 10 wt% Al microparticle and TiO_2 nanoparticle inclusions.

The comparison results of the water collection are presented in Fig. 9 and 10. The weight of the collected water was measured at 20, 40, and 60 min. As presented in Fig. 9, the nanocomposite with 10 wt% micro- and nanoparticles has generally higher water collection performance than the other samples studied here. The poor water collection performance of the PAN/PMMA nanocomposite fibers can be explained by their inherent hydrophobic and water-absorption properties. Due to gravity, the condensed water can wet and saturate the nanocomposite fibers before dripping. The water collection capacity of the four different nanocomposite fibers with different surface wettability is presented in Fig. 10.

The PAN/PMMA nanocomposite fibers exhibited a water collection efficiency of 0.258 g cm^{-2} h^{-1}, whereas, with the incorporation of 2.5 and 5 wt% micro- and nanoparticles, the water collection efficiency went up to 0.411 g cm^{-2} h^{-1} and 0.507 g cm^{-2} h^{-1}, respectively. The highest fog harvesting efficiency among all four different nanocomposite fibers was 0.621 g cm^{-2} h^{-1}, which was that of the PAN/PMMA/10 wt% micro- and nanoparticle sample. The hydrophilic properties of TiO_2 and Al particles can play a positive role in water collection when combined with a superhydrophobic domain. The introduction of TiO_2 and Al micro- and nanoparticles (mainly hydrophilic) ameliorates the fog collection efficiency, which indicates an increase of water coalescence and condensation on those surfaces with superhydrophobic domains. The superhydrophobic surface allows droplets to roll down into the water collecting container more easily instead of adhering and evaporating on the superhydrophilic surface. However, the incorporation of a more hydrophilic ingredient will destroy the original superhydrophobicity of the fibers, which may lead to poor water-collection performance. The superhydrophobic–hydrophilic hybrid surface demonstrates greater fog-collecting performance.

Moreover, the small water droplets that are captured on the hydrophilic regions typically move toward the hydrophobic regions, driven by the wettability differences, and subsequently coalesce into larger droplets in these regions. When the droplets in the hydrophilic regions grow beyond a certain threshold, they drip from the surface by means of gravity.[34] As shown in Fig. 10, the gradual ascent of the water collecting amount indicates the influence that hydrophilic TiO_2 and Al micro- and nanoparticle bumps have on water pinning. The combined effect of the hydrophobicity of the surface and the number of

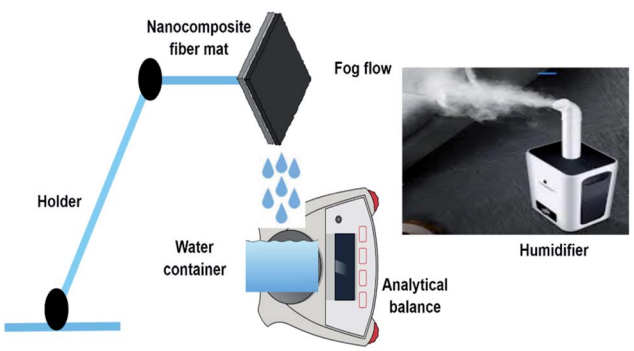

Fig. 8 Illustration of the fog water harvesting system.

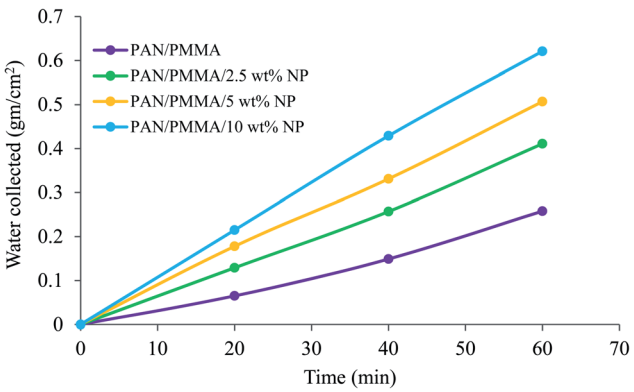

Fig. 9 The amount of water collected using each nanocomposite sample along with collection time.

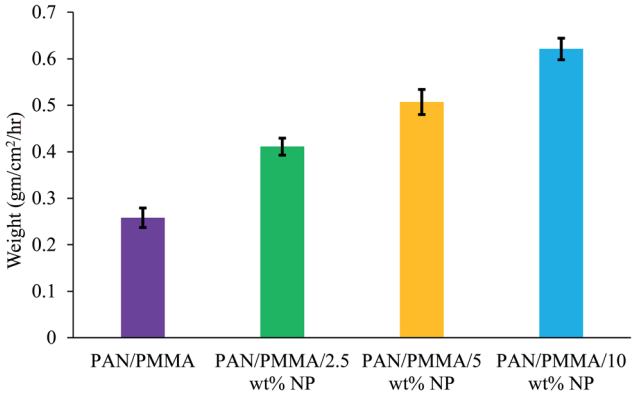

Fig. 10 The total amount of water collected using each nanocomposite sample in 1 h.

hydrophilic ingredients determines the fog-harvesting performance of the nanocomposite fibers. An efficient fog-harvesting nanofiber should have enough hydrophilic sites to adhere to and fix the fog droplets, and integral superhydrophobic properties to accelerate the rolling of water drops. Thus, the nanocomposite fibers with micro- and nanoparticles integrate and balance the surface water droplet coalescence and drainage, which are two competing processes in fog harvesting. The droplet coalescence requires hydrophilicity, whereas droplet drainage benefits from superhydrophobicity. The water condensation and coalescence processes that occur on the nanocomposite fibers were recorded by using a digital camera discretely at 2, 4, and 6 min. The optical images of the fog coalescing behavior on the surface of the nanocomposite fibers are shown in Fig. 11. As can be seen, many droplets formed on the surface at 2 min, and their coalescence was more evident. The gravitational force acting on the droplets increases with the increasing droplet volume.[35] However, the force that resists the mobility of the water droplet depends on the shape and radius of the droplet. The resistance force increases while the radius of the droplet increases.[17] Hence, at an optimum volume of a droplet at which the gravitational force overcomes the resistive force, the droplet roll-off begins. It has been stated that smaller water droplets are mobile and can easily roll off surfaces.[36]

In addition to the significance of the water-capturing (condensation and coalescence) process, the drainage of

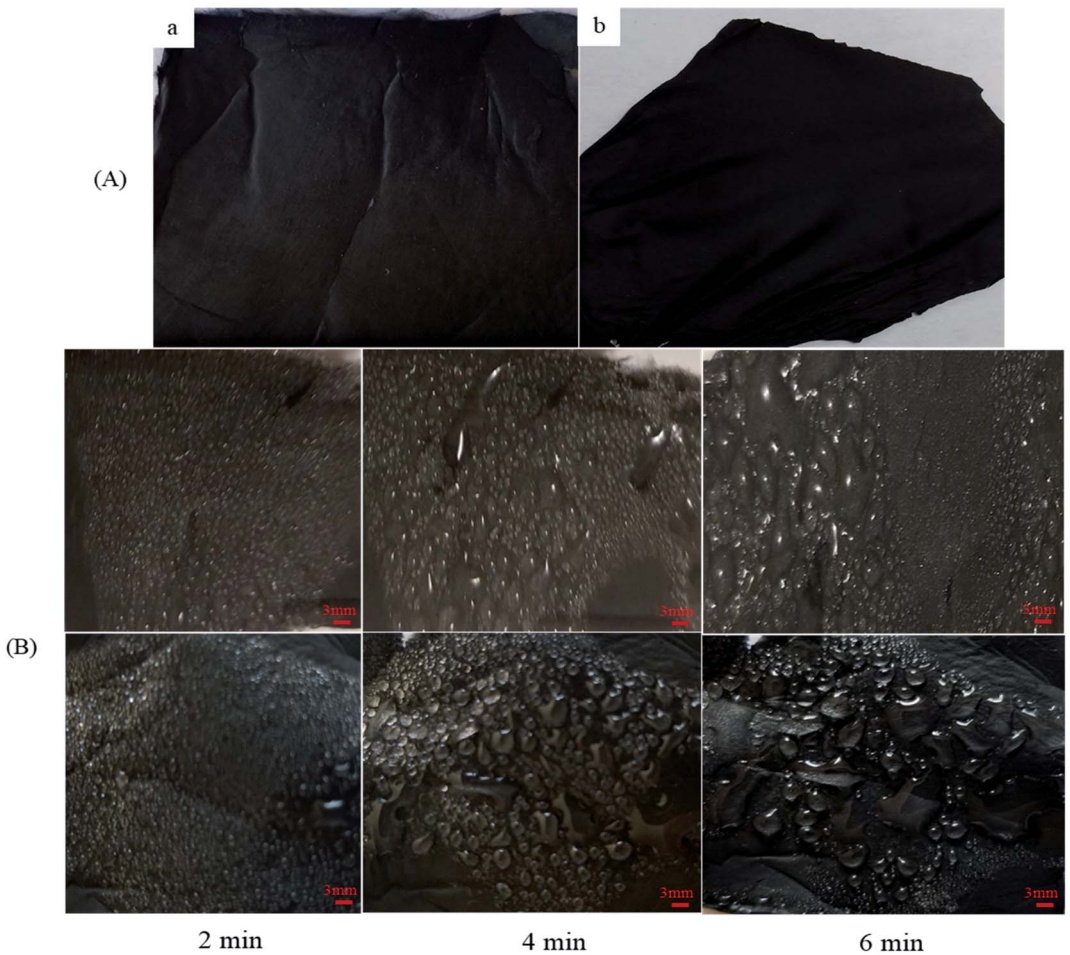

Fig. 11 (A) Optical images of (a) PAN/PMMA and (b) PAN/PMMA/10 wt% NP nanocomposite fibers. (B) Optical images of the fog coalescence process along with time: PAN/PMMA nanofibers (top) and PAN/PMMA/10 wt% NP nanocomposite fibers (bottom).

captured water is also important. An efficient water drainage system means that more water is released in a shorter time. The behavior of droplet growth on the PAN/PMMA and the PAN/PMMA/10 wt% NP nanocomposite fibers is distinctly different. The fog droplet impacting the surface grows by coalescence and subsequently condensation process.[37] The drop impact on PAN/PMMA nanocomposite fibers leads to droplets growing within the sample as Wenzel droplets. However, on the PAN/PMMA/10 wt% NP nanocomposite fibers, impacted water droplets retain the droplet shape and increase in size, as shown in Fig. 11 (bottom). When the droplets reach a threshold volume, they start to roll off the vertical surface and are subsequently collected at the bottom. This increased the fog-harvesting capacity of the PAN/PMMA/10 wt% NP nanocomposite fiber mats. In the presence of superhydrophilic spots, PAN/PMMA/10 wt% NP nanocomposite fibers harvested more and larger water droplets than the PAN/PMMA nanocomposite fibers alone in the same harvesting time. The stability of the performance and reusability of the nanocomposite fibers were studied by multi-cycle water harvesting and water contact angle tests. One cycle of water collection included one hour of the water-collection process using the previously mentioned method, followed by air-drying and also drying in an oven for 30 min at 60 °C. The water contact angle and water collection performance of the PAN/PMMA/10 wt% NP nanocomposite fibers were recorded after 5, 10, and 15 cycles. As shown in Fig. 12 and 13, there was no obvious impairment in the water contact angle or water collection performance, even after 15 cycles of water collection repetition. This is attributed to the good conservation of the superhydrophobicity and TiO_2 and Al nanoparticles on the carbonized nanocomposite fibers. Even after 15 cycles, a stable water collection performance was observed. The combination of hydrophobic and hydrophilic fractions and micro- and nanomaterials with controlled roughness enables the most effective mechanism in water collection.

The fog water harvesting performance of the fabricated nanocomposite fiber mats is compared with the data of other published polymer nanocomposite fibers in the literature. The natural fog harvester, *i.e.*, the desert beetle, has a fog-harvesting efficiency of 21.4 mg cm^{-2} h^{-1}.[38] In comparison to this natural

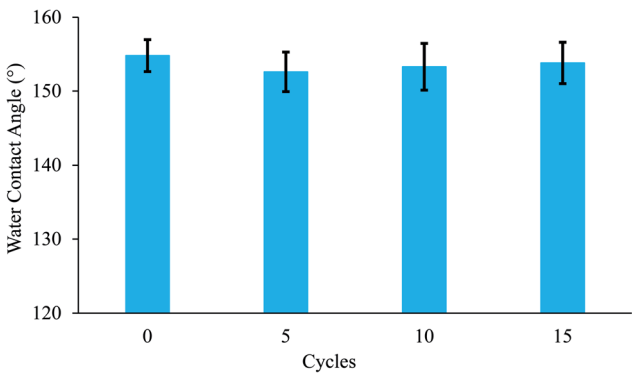

Fig. 12 Water contact angle of PAN/PMMA/10 wt% NP nanocomposite fibers for different water collection cycles.

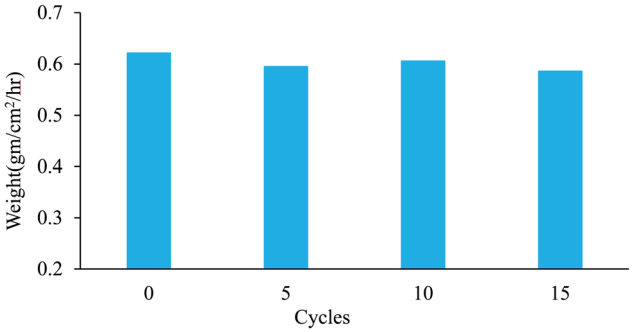

Fig. 13 Water collection of PAN/PMMA/10 wt% NP nanocomposite fibers for different water collection cycles.

fog harvester, our nanocomposite fibers exhibit around 29 times greater harvesting capacity. PVDF/EG composites and fluorinated PAN nanofibers have a collection efficiency of 168.5 mg cm^{-2} h^{-1} and 335 mg cm^{-2} h^{-1}, respectively.[23,24] However, PAN/PMMA/10 wt% NP nanocomposite fibers have a higher water-harvesting capacity compared to previous collectors. Our nanocomposite fibers possess far greater fog water-collection performance than other nanofibers. This can be due to the high surface area and superhydrophobic properties of nanofibers, the combination of micro and nanoparticles forming hierarchical structures, and the presence and hydrophilic and hydrophobic sites on the surface of the fibers. Moreover, the superhydrophobicity of these types of nanocomposites is conserved because of high-temperature carbonization under an inert atmosphere. And long-term durability is expected to be possible because of the good chemical, thermal, and mechanical stabilities of the nanocomposites fibers. With some simplifying assumptions, the material cost which could deliver 6 l of water per day, the minimum daily water requirement for a household with 2 members, was estimated to be $4.96. This fog water harvester is focused on providing clean water to fulfill the minimum water intake requirement in a household with 2 members. The guideline value (*i.e.*, 3 l per day per person) suggested by the WHO was used to roughly estimate the overall investment cost.[39]

4. Conclusions

In summary, we developed an easy and low-cost method for the fabrication of permanent superhydrophobic–hydrophilic nanocomposite hybrid surfaces that provide excellent fog water-collection performance. This inexpensive and facilely fabricated hierarchical assembly bio-mimics the desert beetle back that is capable of highly efficient fog water harvesting without additional energy consumption. The results in this work indicate that the carbonized fibers with 10 wt% nanoparticle inclusions exhibit a water contact angle of 154.8° and daily water productivity of more than 1.49 liter m^{-2} of nanocomposites. It is estimated that the material cost of making such nanocomposites to supply minimum daily water consumption for a household with 2 members (*i.e.*, 6 liters) is only $4.96 (USD). Besides, the nanocomposites could be used repeatedly while the fog water

harvesting performance stayed almost invariant. We believe that due to the high-fog water-harvesting performance and durability, the developed technology has great practical value in large-scale applications. The lower temperature stabilization and higher temperature carbonization process produce high-quality carbon fibers and enhance the surface wettability as well. The process parameters of the stabilization and carbonization process and the nature of precursor fibers influence the properties of the carbon fibers. The experimental results reveal that uniform diameter fibers were produced, and the addition of nanomaterials increased the degree of fiber crystallization. It is safe to conclude that this technology is most likely to have potential application in harvesting fog water on a large scale for water-deficient countries for living and even in agricultural irrigation systems.

Conflicts of interest

The authors declare that there is no conflict of interest concerning the research and authorship of this article.

Acknowledgements

The authors greatly acknowledge Wichita State University for the financial and technical support for the present study.

References

1 K. Onda, J. Lobuglio and J. Bartram, Global Access to Safe Water: Accounting for Water Quality and the Resulting Impact on MDG Progress, *Int. J. Environ. Res. Public Health*, 2012, **9**(3), 880–894.
2 United Nations Convention to Combat Desertification, *Desertification: The Invisible Frontline*, retrived from https://www.unccd.int/sites/default/files/documents/12112014_invisible frontline_ENG.pdf, accessed: Feb. 13, 2020.
3 N. Uddin, M. Alamir, H. Muppalla, M. M. Rahman and R. Asmatulu, Nanomembranes for Sustainable Fresh Water Production Nanomembranes for Sustainable Fresh Water Production, in *International Conference on Mechanical*, Industrial and Energy Engineering, 2018.
4 Y. Zheng, H. Bai, Z. Huang, X. Tian, F. Q. Nie, Y. Zhao, J. Zhai and L. Jiang, Directional Water Collection on Wetted Spider Silk, *Nature*, 2010, **463**(7281), 640–643.
5 A. R. Parker and C. R. Lawrence, Water Capture by a Desert Beetle, *Nature*, 2001, **414**, 33–34.
6 H. G. Andrews, E. A. Eccles, W. C. E. Schofield and J. P. S. Badyal, Three-Dimensional Hierarchical Structures for Fog Harvesting, *Langmuir*, 2011, **27**(7), 3798–3802.
7 J. Ju, H. Bai, Y. Zheng, T. Zhao, R. Fang and L. Jiang, A Multi-Structural and Multi-Functional Integrated Fog Collection System in Cactus, *Nat. Commun.*, 2012, **3**, 1246–1247.
8 M. N. Uddin, F. J. Desai and E. Asmatulu, Biomimetic Electrospun Nanocomposite Fibers from Recycled Polystyrene Foams Exhibiting Superhydrophobicity, *Energy, Ecol. Environ.*, 2020, **5**(1), 1–11.
9 R. Li, Y. Shi, L. Shi, M. Alsaedi and P. Wang, Harvesting Water from Air: Using Anhydrous Salt with Sunlight, *Environ. Sci. Technol.*, 2018, **52**(9), 5398–5406.
10 Z. Wang, M. Elimelech and S. Lin, Environmental Applications of Interfacial Materials with Special Wettability, *Environ. Sci. Technol.*, 2016, **50**(5), 2132–2150.
11 A. Khadak, M. N. Nizam Uddin, M. M. Rahman and R. Asmatulu, Enhancing the De-Icing Capabilities of Carbon Fiber-Reinforced Composite Aircraft *via* Permanent Superhydrophobic Coatings, in *CAMX 2018 – Composites and Advanced Materials Expo*, 2018.
12 M. Salahuddin, M. N. Uddin, G. Hwang and R. Asmatulu, Superhydrophobic PAN Nanofibers for Gas Diffusion Layers of Proton Exchange Membrane Fuel Cells for Cathodic Water Management, *Int. J. Hydrogen Energy*, 2018, **43**(25), 11530–11538.
13 M. N. Uddin, H. T. N. Gandy, M. M. Rahman and R. Asmatulu, Adhesiveless Honeycomb Sandwich Structures of Prepreg Carbon Fiber Composites for Primary Structural Applications, *Adv. Compos. Hybrid Mater.*, 2019, **2**(2), 339–350.
14 M. N. Uddin, J. M. George, V. R. Patlolla and R. Asmatulu, Investigating the Effects of UV Light and Moisture Ingression on Low-Impact Resistance of Three Different Carbon Fiber–Reinforced Composites, *Adv. Compos. Hybrid Mater.*, 2019, **2**(4), 701–710.
15 F. Desai, N. Seyedhassantehrani, M. Shagar, S. Gu and R. Asmatulu, Preparation and Characterization of KOH-Treated Electrospun Nanofiber Mats as Electrodes for Iron-Based Redox-Flow Batteries, *J. Energy Storage*, 2020, **27**, 101053.
16 K. Yin, H. Du, X. Dong, C. Wang, J.-A. Duan and J. He, A simple way to achieve bioinspired hybrid wettability surface with micro/nanopatterns for efficient fog collection, *Nanoscale*, 2017, **9**, 14620–14626.
17 J. Wu, K. Yin, M. Li, Z. Wu, S. Xiao, H. Wang, J.-A. Duan and J. He, Under-oil self driven and directional transport of water on a femtosecond laser-processed superhydrophilic geometry-gradient structure, *Nanoscale*, 2020, **12**, 4077–4084.
18 J.-A. Duan, X. Dong, K. Yin, S. Yang and D. Chu, A hierarchical superaerophilic cone: Robust spontaneous and directional transport of gas bubbles, *Appl. Phys. Lett.*, 2018, **113**, 203704.
19 Y. Wang, L. Zhang, J. Wu, M. N. Hedhili and P. Wang, A Facile Strategy for the Fabrication of a Bioinspired Hydrophilic–Superhydrophobic Patterned Surface for Highly Efficient Fog-Harvesting, *J. Mater. Chem. A*, 2015, **3**(37), 18963–18969.
20 B. S. Lalia, S. Anand, K. K. Varanasi and R. Hashaikeh, Fog-Harvesting Potential of Lubricant-Impregnated Electrospun Nanomats, *Langmuir*, 2013, **29**(42), 13081–13088.
21 Y. Chen, L. Wang, Y. Xue, Y. Zheng and L. Jiang, Bioinspired Spindle-Knotted Fibers with a Strong Water-Collecting Ability from a Humid Environment, *Soft Matter*, 2012, **8**(45), 11450–11454.

22 M. A. K. Azad, T. Krause, L. Danter, A. Baars, K. Koch and W. Barthlott, Fog Collection on Polyethylene Terephthalate (PET) Fibers: Influence of Cross Section and Surface Structure, *Langmuir*, 2017, **33**(22), 5555–5564.
23 Z. X. Huang, X. Liu, S. C. Wong and J. P. Qu, Electrospinning Polyvinylidene Fluoride/Expanded Graphite Composite Membranes as High Efficiency and Reusable Water Harvester, *Mater. Lett.*, 2017, **202**, 78–81.
24 A. Almasian, G. Chizari Fard, M. Mirjalili and M. Parvinzadeh Gashti, Fluorinated-PAN Nanofibers: Preparation, Optimization, Characterization and Fog Harvesting Property, *J. Ind. Eng. Chem.*, 2018, **62**, 146–155.
25 S. M. Saufi and A. F. Ismail, Development and Characterization of Polyacrylonitrile (PAN) Based Carbon Hollow Fiber Membrane, *Songklanakarin J. Sci. Technol.*, 2002, **24**, 843–854.
26 https://www.hindawi.com/journals/ijp/2013/726872/.
27 https://www.researchgate.net/publication/51225005_Photoproduction_of_iodine_with_nanoparticulate_semiconductors_and_insulators/figures?lo=1.
28 X. Ma, C. Yuan and X. Liu, Mechanical, Microstructure and Surface Characterizations of Carbon Fibers Prepared from Cellulose after Liquefying and Curing, *Materials*, 2014, **7**(1), 75–84.
29 V. Goracheva, T. Mikhailova, S. Fedorkina, N. Konnova, M. Azarova and A. Konkin, Thermographic and Thermogravimetric Analysis of the Thermal Behaviour of Polyacrylonitrile Fibres, *Fibre Chem.*, 1974, **5**, 496–498.
30 K. Tse-Hao, D. Tzy-Chin, P. Jeng-An and L. Ming-Fong, The Characterization of PAN-Based Carbon Fibers Developed by Two-Stage Continuous Carbonization, *Carbon*, 1993, **31**(5), 765–771.
31 I. Sas, R. E. Gorga, J. A. Joines and K. A. Thoney, Literature Review on Superhydrophobic Self-Cleaning Surfaces Produced by Electrospinning, *J. Polym. Sci., Part B: Polym. Phys.*, 2012, **50**(12), 824–845.
32 S. C. Thickett, C. Neto and A. T. Harris, Biomimetic Surface Coatings for Atmospheric Water Capture Prepared by Dewetting of Polymer Films, *Adv. Mater.*, 2011, **23**(32), 3718–3722.
33 X. Chen, J. Wu, R. Ma, M. Hua, N. Koratkar, S. Yao and Z. Wang, Nanograssed Micropyramidal Architectures for Continuous Dropwise Condensation, *Adv. Funct. Mater.*, 2011, **21**(24), 4617–4623.
34 A. Lee, M. W. Moon, H. Lim, W. D. Kim and H. Y. Kim, Water Harvest *via* Dewing, *Langmuir*, 2012, **28**(27), 10183–10191.
35 C. W. Extrand and Y. Kumagai, Liquid Drops on an Inclined Plane: The Relation between Contact Angles, Drop Shape, and Retentive Force, *J. Colloid Interface Sci.*, 1995, **170**(2), 515–521.
36 D. Quéré, Non-Sticking Drops, *Rep. Prog. Phys.*, 2005, **68**(11), 2495–2532.
37 T. S. Yu, J. Park, H. Lim and K. S. Breuer, Fog Deposition and Accumulation on Smooth and Textured Hydrophobic Surfaces, *Langmuir*, 2012, **28**(35), 12771–12778.
38 T. Nørgaard, M. Ebner and M. Dacke, Animal or Plant: Which Is the Better Fog Water Collector?, *PLoS One*, 2012, **7**(4), 4–7.
39 WHO, *Guidelines for Drinking-Water Quality*, 4th edn, 2017.

